Defect Characterization in $ZnGeP_2$ by Time -Resolved Photoluminescence

N. Dietz[a], W. Busse[b], H. E. Gumlich[b], W. Ruderman[c], I. Tsveybak[c], G. Wood[a] and K.J. Bachmann[a]

[a]North Carolina State University, Raleigh, NC 27695, [a]Technical University Berlin, and [c]Inrad, Inc., Northvale, NJ 07647

Abstract

The native defect-related optical properties of $ZnGeP_2$ are studied by steady-state and time-resolved photoluminescence. $ZnGeP_2$ crystals grown from the vapor phase by high pressure physical vapor transport (HPVT) and from the melt by gradient freezing (GF) show a broad infrared emission with peak position at 1.2 eV with a decay time constant of a few μs and a faster recombination center peaked at 1.68 eV. The decay transient for the emission at 1.2 eV exhibits features of classical donor-acceptor recombination and is linked to close-pairs that are tentatively associated with germanium-on-zinc antisite donors and zinc vacancy acceptors. Higher energetic luminescence structures at 1.6eV and 1.7eV are revealed after annealing of the $ZnGeP_2$ crystals and are associated with the formation zinc and phosphorous vacancies in the near surface region. $ZnGeP_2$ crystals grown by HPVT from zinc and phosphorus supersaturated vapor compositions show additional emission structure at 1.8 eV and a sharp donor-acceptor emission at 1.778 eV that is related to the presence of additional donor states.

I. Introduction

Zinc germanium phosphide is a chalcopyrite structure semiconductor with a pseudodirect bandgap of ~2.1 eV at room temperature[1]. It has an attractive transparency range[2] from 670 nm to 13 μm and a relatively large second order susceptibility tensor component (d_{36}= 75 pm/V). In view of its substantial positive birefringence of 0.36%, $ZnGeP_2$ as a suitable material for non-linear optical applications in the infrared, e.g., the fabrication of optical parametric oscillators

(OPO) and harmonic generation based on powerful infrared laser sources[3]. In addition to these and other applications in non-linear optics, $ZnGeP_2$ is of interest in the context of nearly lattice matched heteroepitaxy of compound semiconductors on silicon (a[Si] = 5.451 Å, a[$ZnGeP_2$] = 5.465 Å, c/a[$ZnGeP_2$] = 1.97 at room temperature).

The phase relations in the ternary system Zn, Ge, P are presently only incompletely documented[4]. $ZnGeP_2$ single crystals have been grown from the melt by the gradient freezing[4-6] and horizontal Bridgman methods[7]. Also, small $ZnGeP_2$ crystal platelets have been produced by chemical vapor transport methods[8-10]. $ZnGeP_2$ crystals grown from the melt are semiinsulating ($\rho \approx 10^6 \Omega cm$), an exhibit p-type conductivity with carrier mobility between $10 \leq \mu_p \leq 40 cmVs$ at a net acceptor concentration of $10^{10} \leq N_A - N_D \leq 10^{12}$ cm^{-3}, suggesting a high selfcompensations level[11,12].

Steady state photoluminescence investigations revealed a broad emission band with a peak maxima around 1.2eV[13]. The origin of this broad band has remained ambiguous, specially because only the onset of this emission band was known so far. The reported changes in the high energetic shoulder were investigated as a function of composition deviation due to annealing or slightly off stoichiometric during the growth[12,14,15] remain still valid, keeping in mind that the observed shifts of the maxima around 1.3eV might be caused by the cutoff in the photomultiplier assuming an intensity variation of the emission peaked at 1.2eV.

The polarization and excitation dependence in the PL spectra was used by McCrae et al[16] to introduce a defect model based on one AL1 acceptor band with transitions between spin-orbital spitted conduction band states Γ_6, Γ_7 and the AL1 acceptor band, were an additional splitting of the acceptor band was assumed. However, the strong polarization dependence of transitions involving this conduction band states Γ_6, Γ_7 found in modulated reflectance spectroscopic studies[17] are not consistent with the weak polarization dependence in the PL-spectra and the concluded transitions assumed in the defect energy model. The transitions from the spin-orbital splitted valence band (VB) in the AL1 acceptor states, causing the infrared absorption is a not likely assumption considering the intrinsic character of $ZnGeP_2$ which indicates filled acceptor states and a Fermi level close to the middle of the energy gap.

Early EPR measurements on melt-grown crystals support the strong relation of the EPR-signal with an acceptor band[19]. Later photo-induced EPR spectra were related to the P_{Ge} antisite donor[22]. Recent photo-induced EPR measurements on melt-grown crystals reveal a deep acceptor band associated with Zn vacancies within the surface region probed by this method[23]. Also, ENDOR measurements identified the zinc vacancy as the dominant deep acceptor in bulk ZnGeP crystals grown by directional solidification[24].

In a DA recombination process, after generation of electron-hole pair, the electrons and holes are captured by ionized donors and acceptors. The localized carrier that are separated by a distance, r, may recombine radiatively emitting photons with a energy of

$$h\nu = E_G - (E_D + E_A) + \frac{e^2}{\varepsilon} - \frac{e^2}{\varepsilon}\frac{\alpha^5}{r^6} \quad , \quad (1)$$

where E_G is the band gap energy, E_D and E_A the donor and acceptor binding energies, ε the static dielectric constant and α the effective van der Walls coefficient. For very close pairs, the last term of Equ. (1) results in a series of sharp emission lines. However, a large amount of statistically distributed closely spaced pairs may broaden or even suppress the discrete emission lines to due random strain.

Results and Discussion

The energy resolved steady-state PL data in the energy range from 0.7 eV up to 2.5 eV were obtained using a combination of two liquid-N_2 cooled detectors, a GaInAs photomultiplier tube (PMT) and a Ge diode in conjunction with a 0.5m single-grating monochromator. The excitation was accomplished by an Ar laser with excitation energies of 2.7eV (λ=457.8nm), 2.54eV (λ=488nm) and 2.4eV (λ=514.8 nm) excitation lines. The system responds of the PMT was corrected to allow the combination of the two spectra, which is essential since the decreasing response of the PMT below 1.3 eV results in a false peak position of the infrared luminescence near 1.3 eV. Time-resolved PL data were obtained by time-correlated single-photon counting technique. The excitation energy was varied by a XeCl pumped (Eximer laser λ=308nm) Dye laser system, Lamda EMG53MSC, in the wavelength range 460-510nm (Coarin102). The output of the Dye laser was controlled by neutral-filters with a incident power between 100 mW and 3Watt and repetition rates between 200Hz and of 50Hz, respectively. The pulse width is in the

order of 18ns. The resulting luminescence was collected and focused in a double monochromator and detected with an S-1 PMT. In lack of fast response detectors in the infrared region below 1.2 eV, the time dependence of the luminescence is carried out only in the energy range from 1.2eV up to 1.8 eV.

Figure 1 shows a typical PL spectrum for an as-grown $ZnGeP_2$ cut from a bulk single crystal grown by the gradient freezing (GF) method. The spectrum is build up from two PL spectra taken with a PMT (1.2eV up to 2.5 eV) and a Ge-diode (0.7eV up to 1.3 eV). In the energy range 1.0eV up to 2.0eV the spectrum is corrected with the of the PMT and the Ge-diode response function. Below 1.0 eV no correction function for the monochromator and Ge diode response was available. Thus obtained PL spectrum is dominated by the emission peak at 1.2eV with two high energetic shoulders around 1.58eV and 1.68eV. The luminescence of all $ZnGeP_2$ samples show a very strong temperature dependence and no luminescence is detected at room temperature. Figure 2 shows the temperature dependence of the PL spectrum for $ZnGeP_2$ bulk crystal. With increasing temperature the high energetic emission around 1.6e V and 1.7eV decreases rapidly leaving at 100K the 1.3 eV emission as dominant feature.

The time dependence of the observed emission structures in bulk crystals is shown in Figure 3. The spectra are obtained with a S1-PMT in the single-photon counting mode and are not corrected with the PMT response characteristic. The upper curve in fig. 3 shows the emission spectrum of an annealed $ZnGeP_2$ crystal taken without a time window. The emission spectrum obtained in the time window from 0 to 100 μs contains only the high energetic emission structure at 1.68 eV with a small contribution around 1.3-1.4 eV. The emission spectra taken in the time windows 0.1-2ms, 2-18ms and 18-65ms show only one emission contribution with a constant peak maximum around 1.3eV. This suggest that the broad emission structure at 1.3 eV is correlated to one transition center. Note, that the peak maximum position is falsed by the cutoff edge of the PMT, as indicated in fig. 1. The decay character analyzed in the energy range of 1.2eV to 1.9 eV is shown in fig. 4 in a double logarithmic plot for the emission at 1.326 eV, 1.45 eV, 1.574 eV and 1.698 eV in curve (1), (2), (3) and (4), respectively. The decay transients in the energy range 1.2 eV up to 1.7 eV are fitted with the hyperbolic equation

$$I_{(t)} = \alpha \times \frac{1}{t^{\tau}} \qquad (2)$$

with α as a pre-factor and τ the hyperbolic decay factor.

The decay factor τ changes form τ=0.81 at 1.326 eV to τ=1.0, τ=1.25 and τ=1.6 at , 1.45 eV, 1.574 eV and 1.698 eV, respectively. The parabolic decay time characteristic of the emission can be interpreted in terms of transitions between donor and acceptor states associated with energy subbands in the bandgap of $ZnGeP_2$. The broad PL band, peaked at 1.2 eV, is attributed to transitions between filled acceptor (A1) and unfilled donor (D1) states that are associated with subbands having a center distance of 1.2 eV.

The changes in the emission due to annealing of $ZnGeP_2$ bulk crystals are shown in Figure 5, where the first curve represent the spectrum for an as-grown crystal. Annealing in vacuum for several hundreds of hours at 500°C results in an increase of the high-energetic PL-structures at 1.6eV and a substantial increase of the 1.68eV emission, as shown in curve 2. In order to check whether the annealing changes homogenous the defect properties in the bulk crystal, we removed a layer of ~1μm from the surface of the annealed sample causing a significantly reduction of the high energetic emissions around 1.6 and 1.7 eV (curve 3).

Crystal platelets were grown by horizontal HPVT from molten $ZnGeP_2$ sources with and without additions of excess Zn_3P_2 to cover the entire range of compositions across the homogeneity range of $ZnGeP_2$ from Zn-rich to Zn-deficient vapor. The temperature at which nucleation and growth occurred was ~35°C below the melting temperature. For a stationary molten source, the preferentially evaporation of constituents, e.g. Zn, results in their gradual depletion. In this case, starting under zinc-supersaturated conditions, the composition of the platelet crystals at the position near to their initial nucleation sites at the fused silica wall corresponds to maximum zinc activity in the $ZnGeP_2$ crystal, changing to to lower zinc activity and higher germanium activity in the compound for the periferal parts that are formed in later stages of growth at lower Zn partial pressure. Thus different regions of the homogeneity range may be probed for the same crystal depending on the position of the exciting laser beam.

Figure 6 show photoluminescence spectra obtained for such a crystal plate that is bound by (112) as the largest facets. In the periferal parts of the plate the luminescence is dominated by 1.3 eV emission that is observed in all $ZnGeP_2$ crystals, irrespective of the growth method, albeit at different relative intensity to other emission features that depend on the method of growth and on the detailed history of the samples. Close to the nucleation point an additional emission structure at 1.77 eV is added, as shown in curve 2.

Figure 7 shows the photoluminescence spectra obtained in the center of a platelet with different time windows. The emission spectra are similar to that observed for bulk $ZnGeP_2$ (fig. 3) with one additional sharp emission peaked at 1.778 eV.

The decay time of the emission in the energy range 1.2eV upto 1.6eV is linear in a double logarithmic plot as show in fig. 8. Figure 9(a) shows an enlargement of the emission around 1.778 eV with the decay time plotted in a double log. scale in fig. 9(b).

Although the point defect chemistry is complex, hints for the predominance of certain defects are obtained by the analysis of the annealing behavior and the behavior associated with specific growth conditions. In agreement with the suggestion of Rud and Masagutova[21] we attribute the residual absorption in the transparency range of $ZnGeP_2$ to transitions from the A1 subband into the conduction band and the D1 donor band. From the extension of the absorption to ~ 5 μm, we can conclude that the lower edge of the D1 band extends to ~ 0.25 eV above the upper edge of the A1 band, placing the lowest states belonging to the D1 subband at ~ 1.35 eV below the CBE. Thus, in the absence of other point defects, the FL is pinned to a position between the A1 and D1 subbands in the lower half of the bandgap of $ZnGeP_2$, explaining the high resistivity p-type conductivity. Of course, the presence of additional donors and acceptors that are unrelated to the D1 and A1 subbands can contribute to the residual absorption due to both additional A-D transition pathways and the associated shift in the FL that affects the concentrations of filled acceptor and unfilled donor states.

The transitions between filled A1 and empty D1 states do not contribute to the PC spectra because of the large effective mass in the D1 subband due the localization of the associated donor states. The above interpretation is reinforced by the time-dependent recombination behavior starting with fast high energy transitions related to D-A pairs in close proximity that are

followed by slower recombination at lower energies corresponding to larger separations between the localized D-A pairs.

There are at least three effects that must be considered in the interpretation of the annealing studies: (i) The reduction of quenched-in disorder, reducing the concentration of point defects. (ii) The shift of the FL position associated with this annihilation of defects, altering the population of the remaining defect states. (iii) Shifts in the FL position caused by the generation of defects at the crystal surface upon annealing. The observation of additional structure at higher energy in the PL and the depth dependence of the luminescence features after annealing clearly establishes additional point defect generation at the surface followed by diffusion into the subsurface region.

We note that deviations from stochiometry affect via the mass action law the concentrations of both the antisite defects and vacancies. Consequently E_F depends on both the growth and annealing conditions. In particular, regardless of the as-grown composition, annealing in vacuum depletes the near surface region with regard to the most volatile constituents, that is, phosphorus and zinc. By the mass action law, the formation of vacancies on the zinc sublattice reduces the concentration of Zn_{Ge} acceptors and enhances the concentration of Ge_{Zn} donors according to the reactions [1]: $V_{Zn} + Zn_{Ge} \rightarrow Zn^x$ and [2]: $V_{Zn} + Ge^x \rightarrow Ge_{Zn}$. The introduction of V_P donors at the surface is associated with the formation of and Ge_P acceptors according to the reaction [3]: $V_P + Ge^x \rightarrow Ge_P$, and possibly, but not necessarily, of Zn_P acceptors. Thus the luminescence at 1.6 and 1.7 eV may be explained tentatively by transitions from V_P donors to V_{Zn} and Ge_P acceptors, respectively. The overall FL shift associated with the generation of V_P and V_{Zn} depends on the values of the equilibrium constants for reactions [1] - [3], which are not known at present. The high p-type conductivity observed upon annealing in zinc vapor, has been explained by Rud as an effect of Zn_P antisite defect formation[12].

A more definitive control of the stoichiometry of $ZnGeP_2$ is obtained by growth from the vapor phase. Thermochemical calculations of the temperature dependence of the existence range of $ZnGeP_2$ show that HPVT of $ZnGeP_2$ from a molten source ties at the lower substrate temperature into solidus compositions close to the boundary between the $ZnGeP_2$ and ZnP_2 of the $ZnGeP_2$ existence range[25]. The n-type conductivity of $ZnGeP_2$ crystals grown under such

conditions suggests the formation of relatively shallow donor states that move the FL toward the conduction band edge. The high phosphorus pressure used in these experiments rules out a higher V_P concentration than observed under the conditions of melt growth. Thus the donor responsible for the 1.8 eV emission for HPVT growth from a zinc supersaturated vapor phase must be associated with a different point defect that does not form under for HPVT growth from zinc-depleted melt compositions. Possible choices are the P_{zn} and P_{Ge} antisite defects of which only the P_{Ge} donor explains the decrease of the intensity of the 1.8 eV emission with decreasing zinc activity in the solid. Therefore, we associate the relatively shallow donor that is formed upon HPVT growth from a phosphorus and zinc supersaturated vapor phase with the P_{Ge} antisite defect.

Further information is gained from the analysis of optical brightening in conjunction with the PL results. The broad deep luminescence in $ZnGeP_2$ crystals observed for crystals grown from zinc-depleted nutrients is due to close-spaced D-A pairs of variable spacings, corresponding to broad donor and acceptor subbands. Accepting the interpretation of ref. 24, the deep acceptor is associated with V_{zn}. By equation 2 it is in turn associated with the Ge_{Zn} antisite defect, so that the Ge_{Zn}-V_{Zn} close-spaced D-A pairs represent a possible choice. The alternative close-pairing V_P-V_{Zn} has been proposed in ref. 19 on the basis of the photo-induced EPR study. Unfortunately the photo-induced EPR emloying HeNe laser radiation probes only a thin surface region of the $ZnGeP_2$ crystal, which is expected to be depleted of Zn and P. Thus the finding of both V_P and V_{zn} by photo-induced EPR, though being in agreement with other evidence referer-ring to the near surface region, does not necessarily pertain to the optical brightening upon annealing, which is a bulk effect. We prefer the Ge_{Zn} donor since it provides for the simul-taneous elimination of V_{Zn} and Ge_{Zn} sites upon annealing according to the reaction [4]: $Ge_{Zn} \rightarrow Ge^x + V_{zn}$ and the mass action law, which may be further enhanced by a simultaneous reduction of cation disorder on the Ge sublattice, that is, Zn_{Ge} according to [5] $Zn_{Ge} + V_{zn} \rightarrow Zn^x$. The associated FL motion toward the conduction band edge that results in the filling of residual deep Ge_{Zn} donor states by electrons further enhances the optical brightening. Of course, the simultaneous elimination of P- and Zn-vacancies upon annealing would be also possible, but there exists no obvious linkage in this case. Also, we note that the formation of Ge_{Zn}-V_{Zn} pairs

can explain the observed increase in the P-P bond angle[24], which is not the case for V_P-V_{Zn} pairing.

Conclusion

The native defect-related optical properties of $ZnGeP_2$ were studied by steady-state and time-resolved PL. The decay transients for the emission the energy range 1.2 - 1.6eV show hyperbolic behavior which is interpreted as donor-acceptor pair recombination. Higher energetic luminescence structures at 1.6eV and 1.7eV were revealed after annealing of the $ZnGeP_2$ crystals and assigned to the formation Zn- and Phosphorous vacancies in the near surface region upon annealing. $ZnGeP_2$ crystals grown from a phosphorus and zinc supersaturated vapor phase show additional emission structure at 1.8 eV and a sharp donor-acceptor emission at 1.778 eV that is related to the presence of additional donor states. The deep luminescence observed for crystals grown from the melt and from zinc depleted vapor sources is related to close pair D-A transitions between subbands associated with the Ge_{Zn} and V_{Zn} defects. The bulk optical brightening effect is explained as the simultaneous elimination of V_{zn} and cation disorder upon annealing.

Acknowledgments

This work has been supported by NSF grants DMR 9202210 and SBIR No. III-9316988 and NASA grant NAGW-2865.

References:

[1] J. L. Shay and J. H. Wernick, Academic Press, New York (1976).

[2] G. D. Boyd, H. M. Kasper, J. H. McFee and F. G. Storz, IEEE J. Quantum. Electron. QE 8, 900 (1972).

[3] Y. M. Andreev, V. G. Voevodin, A. I. Gribenyukov and V. P. Novikov, Sov. J. Quantum. Electron. 17, 748 (1987).

[4] E. Buehler, J. H. Wernick and J. D. Wiley, J. Electron. Mater. 2, 796 (1973).

[5] A. S. Borshchevskii, N. A. Goryunova, F. P. Kesamanly and D. N. Nasledov, physica status solidi **21**, 9-55 (1967).

[6] B. Ray, A. J. Payne and G. J. Burnell, phys. stat. sol. **35**, 197-204 (1969).

[7] G. C. Xing and K. J. Bachmann, Appl. Phys. Lett. 56(3), 271 (1990).

[8] S. A. Mughal, A. J. Payne and B. Ray, Journal of Materials Science **4**, 895-901 (1969).

[9] M.S. Shen et al., J. Sol. St. Chem. 71, 176 (1987).

[10] Y. G. Kataev, I. A. Bobrovnikova, V. G. Voevodin, E. I. Drigolenko, L. G. Nesteryuk and M. P. Yakubenya, Soviet Physics Journal (Izvestiya Vysshikh Uchebnykh Zavedenii, Fizika) **4**, 74-78 (1988).

[11] G. Balcaitis, Z. Januskevicius and A. Sodeika, phys. stat. sol. **(a) 89**, K71-K74 (1985).

[12] Yu. V. Rud, Semiconductors **28**(7) p.633-655 (1994).

[13] N. Dietz, I. Tsveybak, W. Ruderman, G. Wood and K.J. Bachmann, Appl. Phys. Lett. **65** (22) p. 2759 (1994).

[14] G. K. Averkieva, V. S. Grigoreva, I. A. Maltseva, V. D. Prochukhan and Y. V. Rud, phys. stat sol. (a) **39**, 453-457 (1977).

[15] H. M. Hobgood, T. Henningsen, R. N. Thomas, R. H. Hopkins, M. C. Ohmer, W. C. Mitchel, D. W. Fischer, S. M. Hegde and F. K. Hopkins, J. Appl. Phys. 73(8) 4030-7 (1993).

[16] J. E. McCrae Jr., M. R. Gregg, R. L. Hengehold, Y. K. Yeo, P. H. Ostdiek, M. C. Ohmer, P. G. Schunemann and T. M. Pollak, Appl. Phys. Lett. 23(6), 3142-4 (1994).

[17] J. L. Shay, B. Tell, E. Buehler and J. H. Wernick, Phys. Rev. Lett. 30(20), 983-6 (1973).

[18] M.H. Rakowsky, W.K. Kuhn, W.J. Lauderdale, L.E. Halliburton, G.J. Edwards, M.P. Scripsick, P.G. Schunemann, T.M. Pollak, M.C. Ohmer, andF.K. Hopkins, Appl. Phys. Lett. 64(13), 1615-17 (1994).

[19] A. Kiel, Solid State Communications 15, 1021-24 (1974).

[20] G. Wood, Master Thesis, North Carolina State University, Raleigh NC 27695 (1994).

[21] Y. V. Rud and R. V. Masagutova, Sov. Tech. Phys. Lett. 7, 72 (1981).

[22] U. Kaufmann, J. Schneider and A. Rauber, Appl. Phys. Lett. 29, 312 (1976)

[23] N.C. Giles, L.E. Halliburton, P. Schunemann and T.M. Pollack, Appl. Phys. Lett. 66, 1758 (1995)

[24] L.E. Halliburton, G.J. Edwards, M.P. Scripsick, M.H. Rankowsky, P.G. Schunemann and T.M. Pollack, Appl. Phys. Lett. 66, 2670 (1995)

[24] S. Fiechter, H. Castleberry, N. Dietz, K.J. Bachmann, H.T. Tran, K. Ito, and J.S. Scroggs, Proc. 7th Int, Symp. on Exp. Methods of Microgravity, R.A. Schiffmann, ed.,TMS, Warrendale, PA, 1995, p. 57

Figure caption:

Figure 1: Photoluminescence spectrum of bulk ZnGeP2 crystal wafers that are cut from a crystal grown by gradient freezing method

Figure 2: Temperature dependence of the emission of bulk $ZnGeP_2$ crystal.

Figure 3: Time dependence of photoluminescence of a bulk $ZnGeP_2$ crystal.

Figure 4: Decay transients of the PL emission at 1.326 eV curve (1), 1.45 eV curve (2), 1.574 eV curve (3) and 1.698 eV curve (4). The exponent τ in the hyperbolic approximation changes form τ=0.81, τ=1.0, τ=1.26 to τ=1.60 for curve (1), (2), (3) and (4), respectively.

Figure 5: Changes in the emission spectra upon back etching of an annealed bulk $ZnGeP_2$ crystal. Curve (1) as-grown $ZnGeP_2$ crystal; (2) after annealing in vacuum for 500h and (3) after back-etching of $\approx$1 μm of the top surface layer.

Figure 6: Photoluminescence spectrum of a HPVT grown $ZnGeP_2$ platelet. The PL spectrum below 1 eV is not corrected. Curve (2) represent the additional emission as it is observed close to the stem of the platelet and is enlarged by a factor of 10.

Figure 7: Time dependence of the emission in the center of a HPVT grown $ZnGeP_2$ crystal..

Figure 8: Decay transients of the PL emission at 1.326 eV curve (1), 1.45 eV curve (2), 1.574 eV curve (3) and 1.698 eV curve (4). The exponent τ in the hyperbolic approximation changes form τ=0.81, τ=1.0, τ=1.26 to τ=1.60 for curve (1), (2), (3) and (4), respectively.

Figure 9: (a) Enlarged emission spectrum around 1.77 eV with (b) the decay transients of emission at 1.7784 eV and 1.7808 eV. Two different hyperbolic decay constants have to be assumed to fit the spectrum.

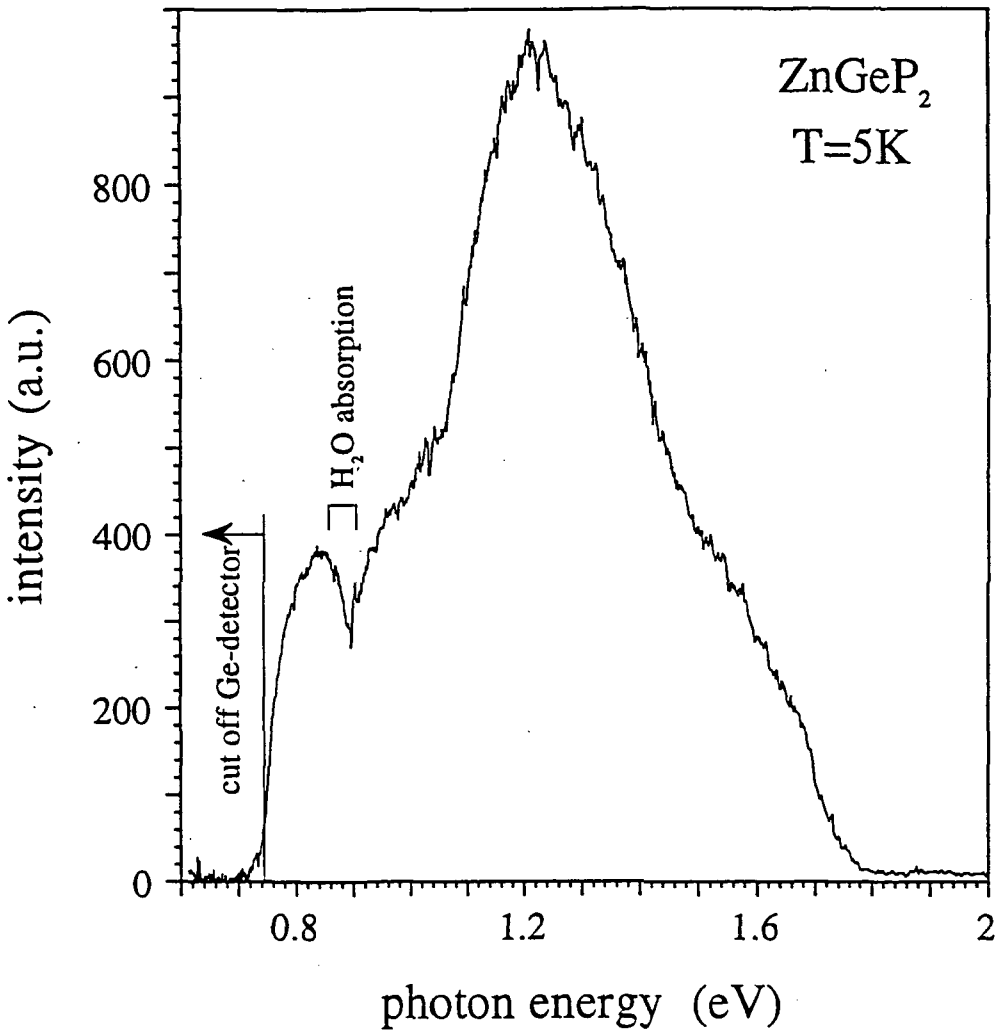
ZnGeP2
T=5K
intensity (a.u.)
0
200
400
600
800
0.8
1.2
1.6
2
photon energy (eV)
cut off Ge-detector
H2O absorption

Fig. 1

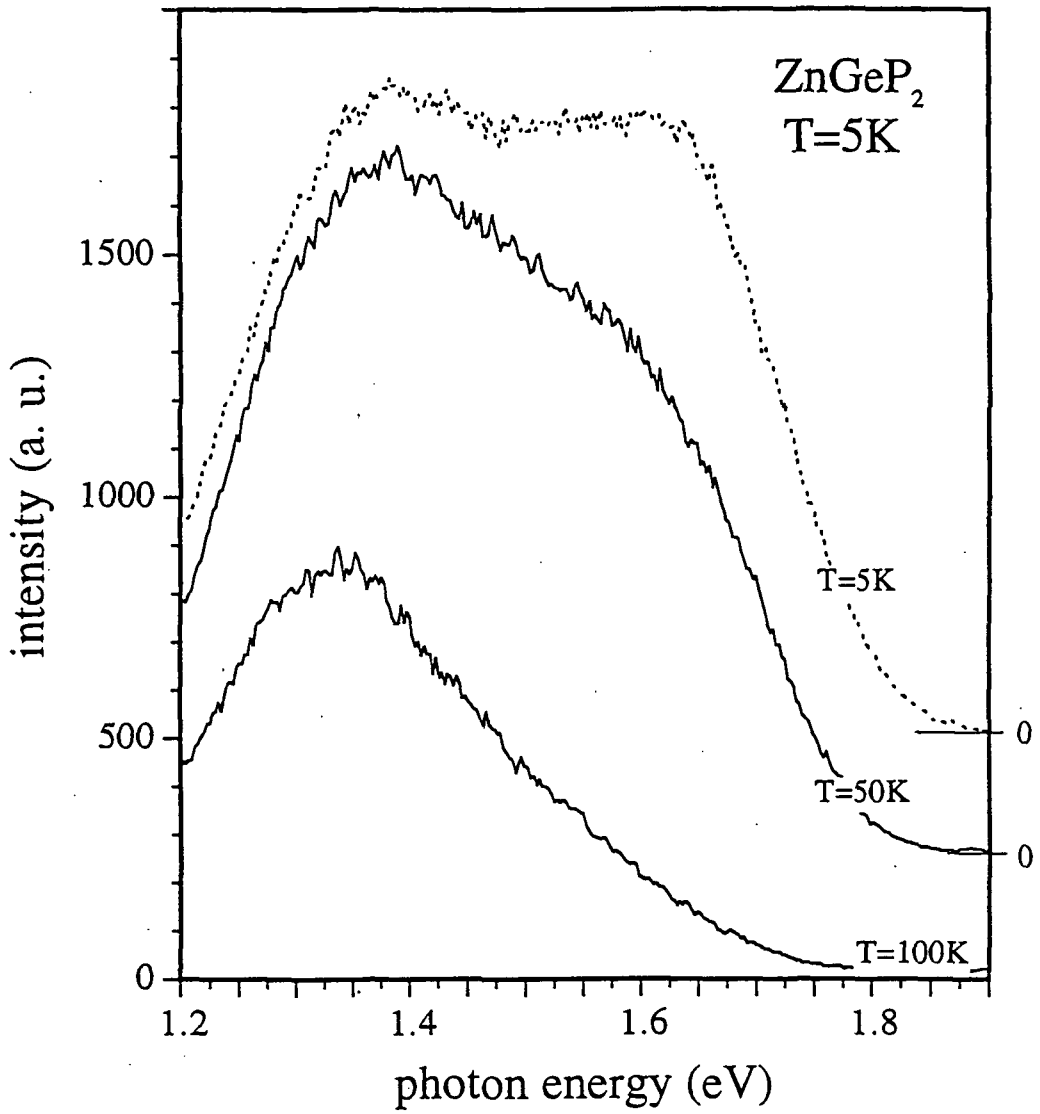
ZnGeP2
T=5K
1500
1000
500
0
intensity (a. u.)
T=5K
T=50K
T=100K
0
0
1.2
1.4
1.6
1.8
photon energy (eV)

Fig. 2

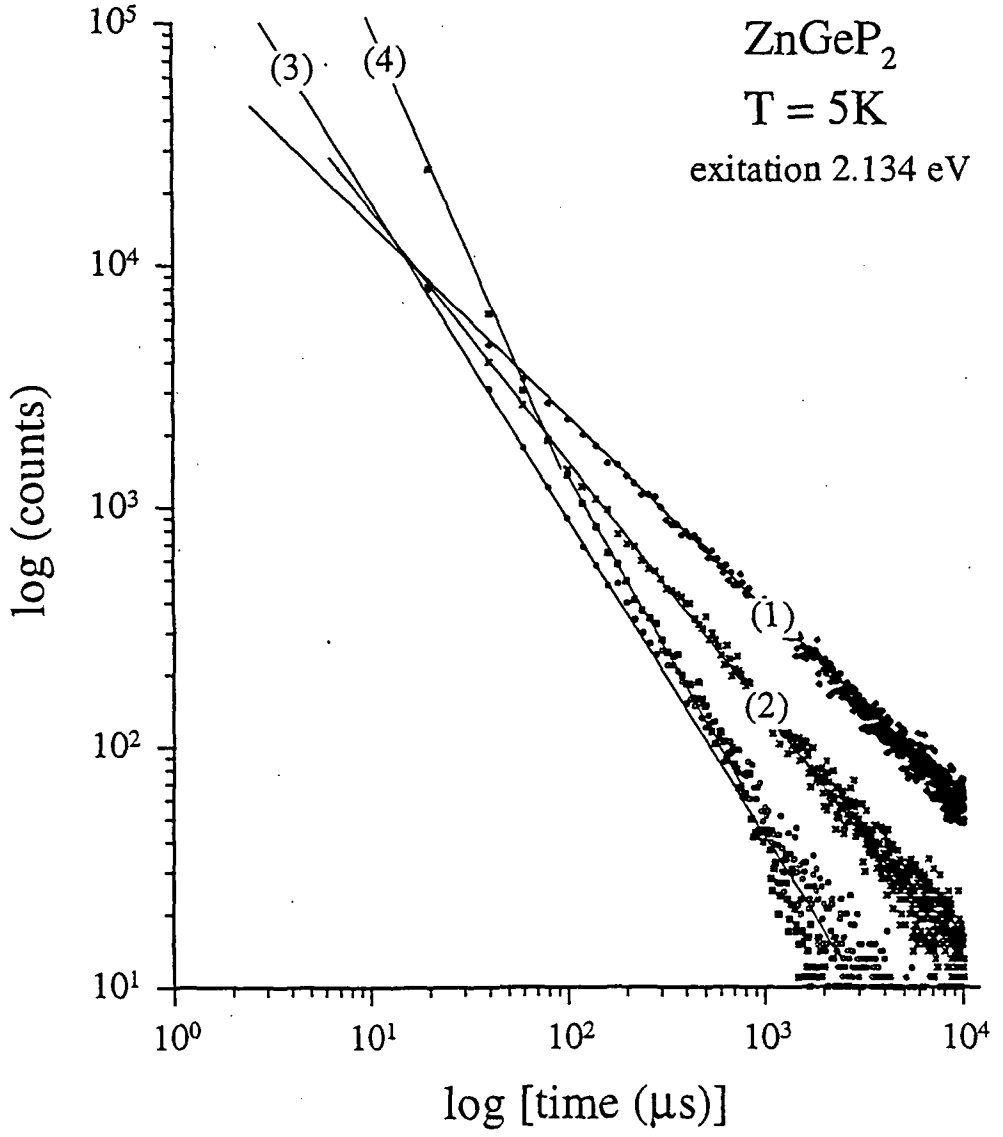

Fig. 4

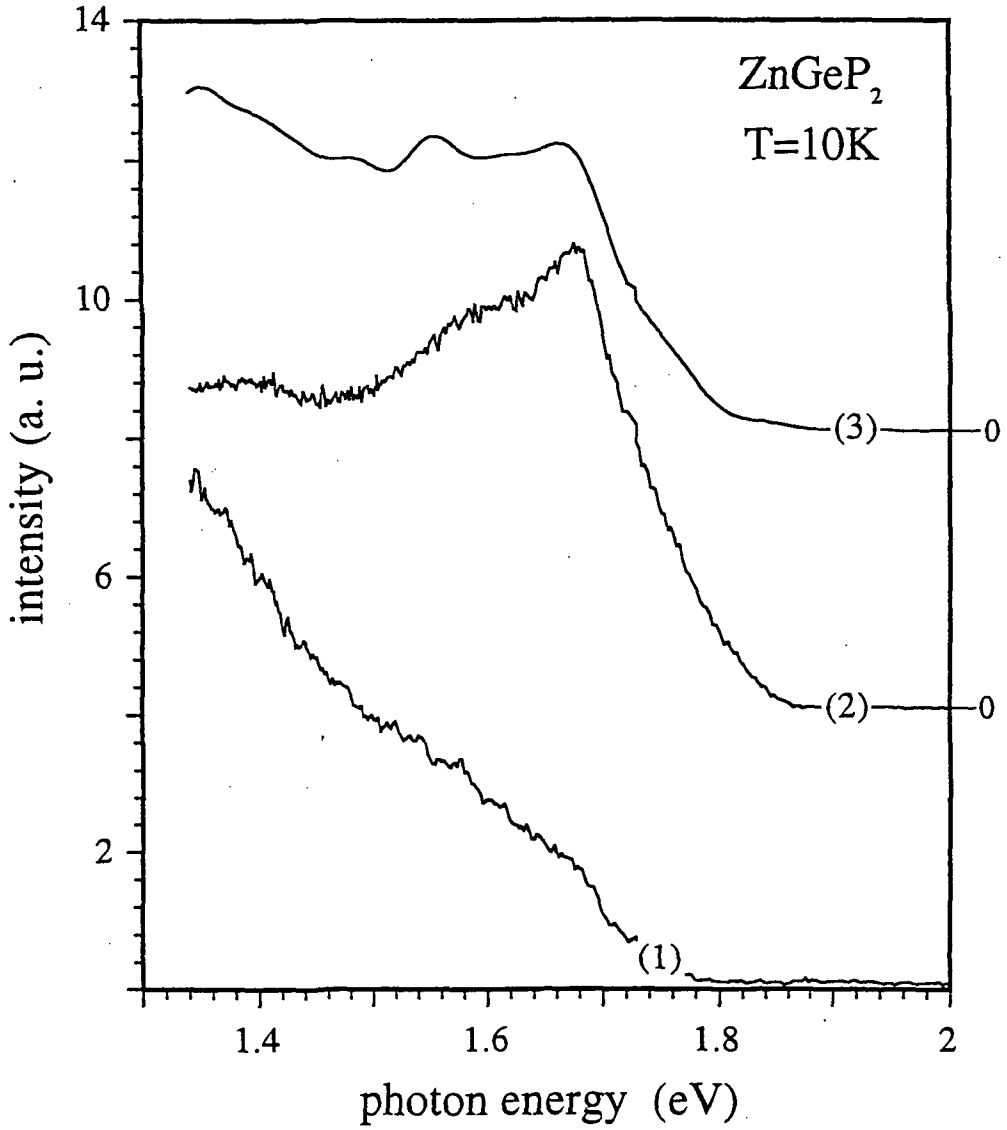
14
10
6
2
intensity (a. u.)
ZnGeP2
T=10K
(3)
0
(2)
0
(1)
1.4
1.6
1.8
2
photon energy (eV)

Fig. 5

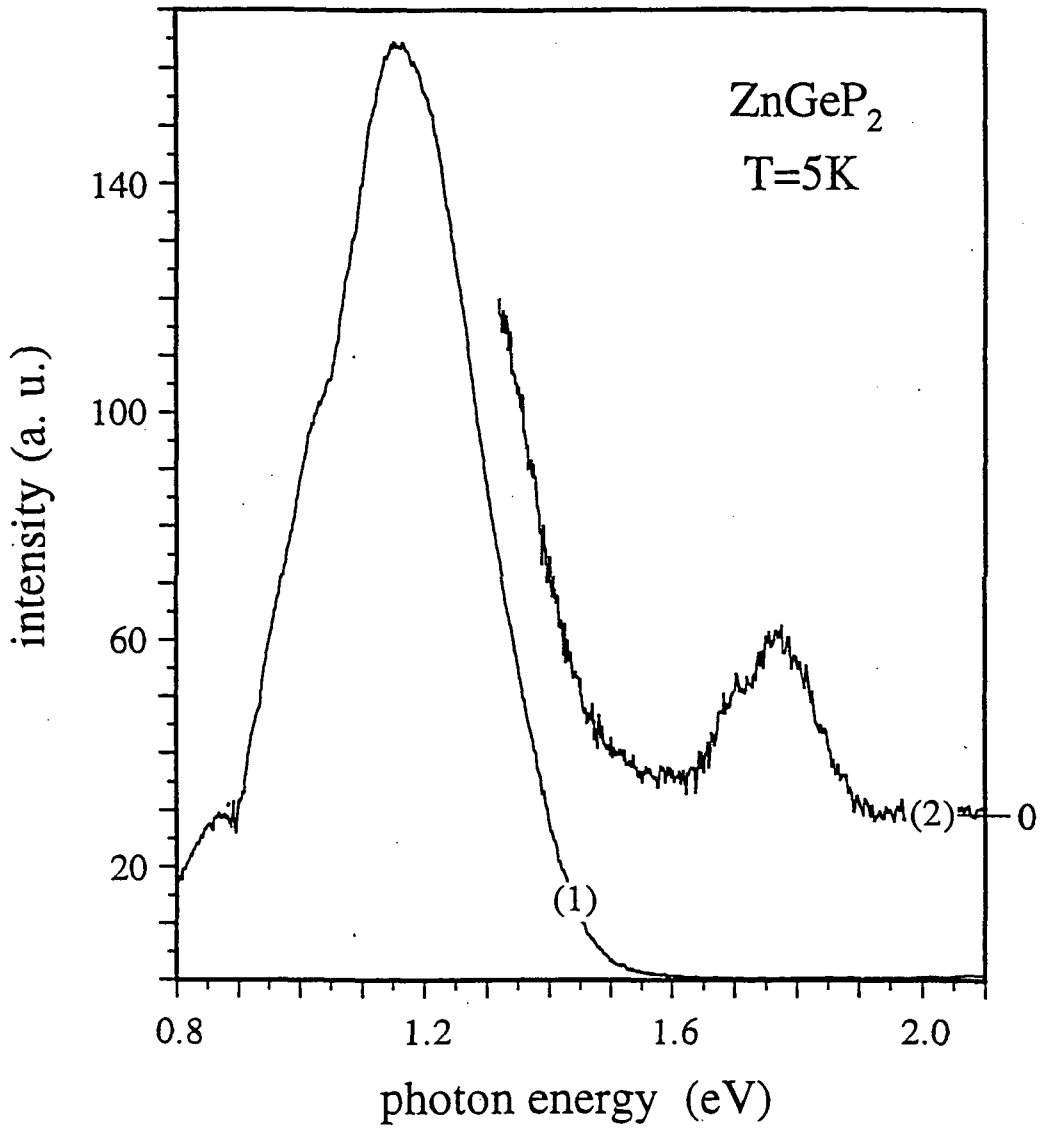
ZnGeP2
T=5K
intensity (a. u.)
140
100
60
20
0.8
1.2
1.6
2.0
photon energy (eV)
(1)
(2)
0

Fig. 6

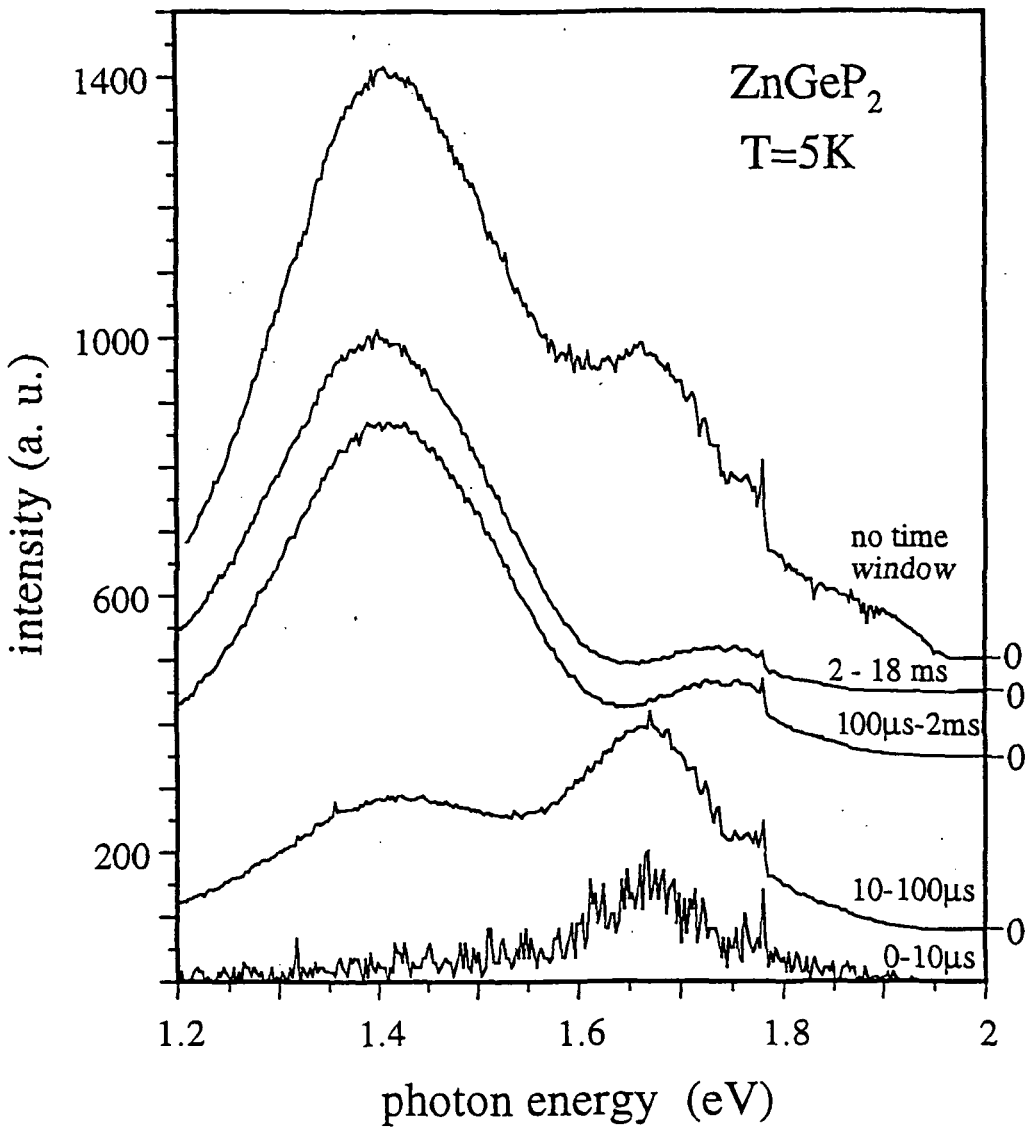
ZnGeP2
T=5K
1400
1000
600
200
intensity (a. u.)
no time window
2 - 18 ms
100µs-2ms
10-100µs
0-10µs
0
0
0
0
1.2
1.4
1.6
1.8
2
photon energy (eV)

Fig. 7

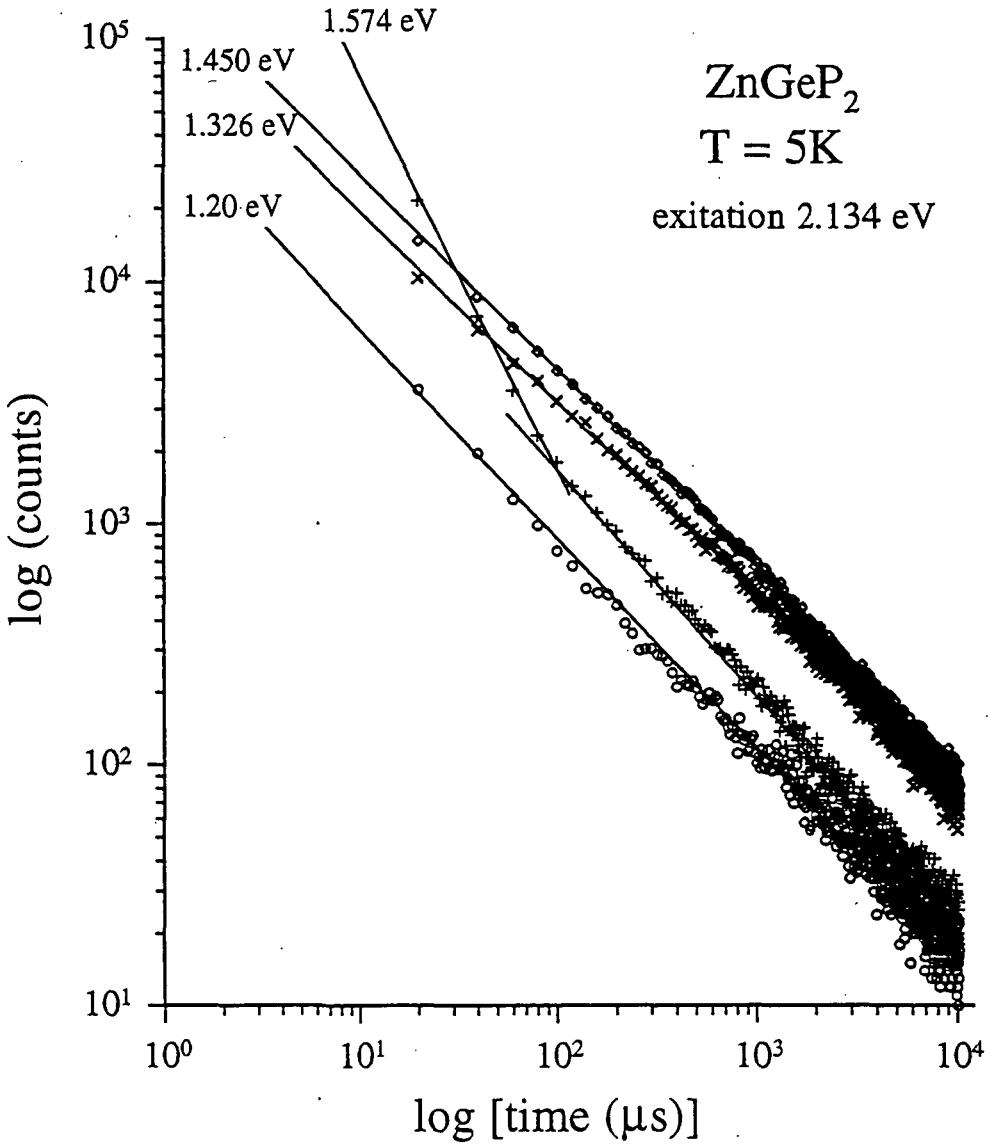
1.574 eV
1.450 eV
1.326 eV
1.20 eV
ZnGeP2
T = 5K
exitation 2.134 eV
log (counts)
log [time (μs)]
10^5
10^4
10^3
10^2
10^1
10^0
10^1
10^2
10^3
10^4

Fig. 8

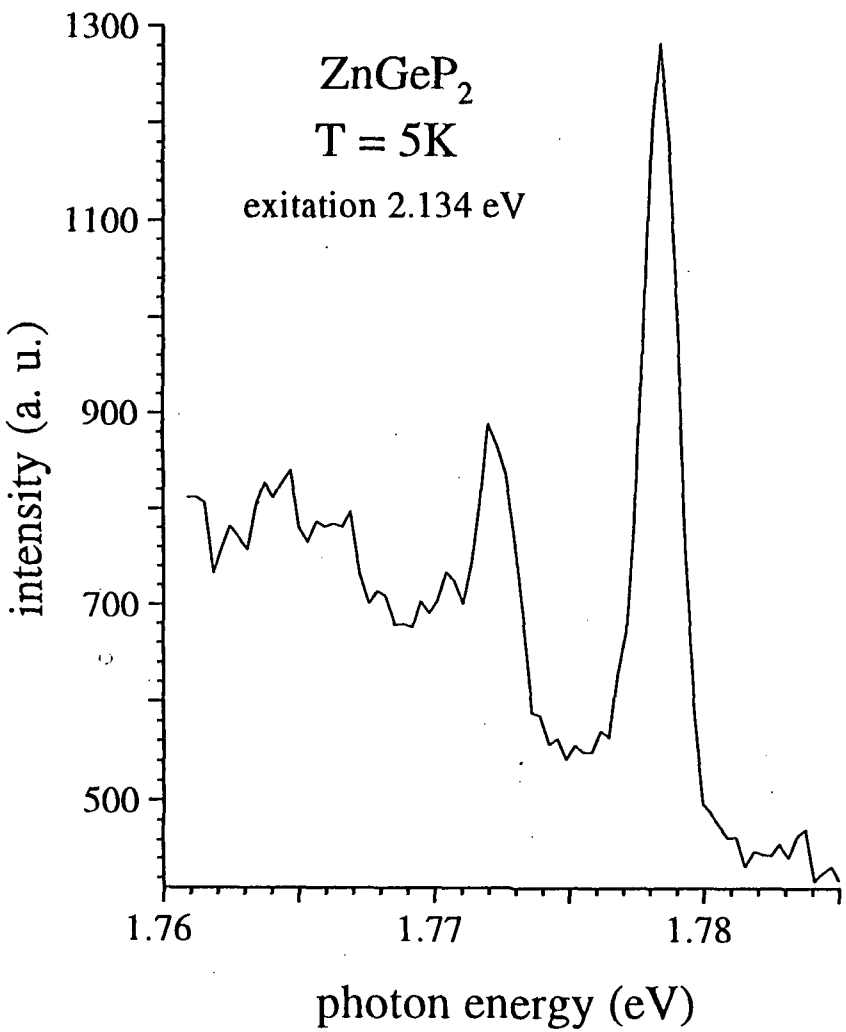
ZnGeP2
T = 5K
exitation 2.134 eV
intensity (a. u.)
1300
1100
900
700
500
1.76
1.77
1.78
photon energy (eV)

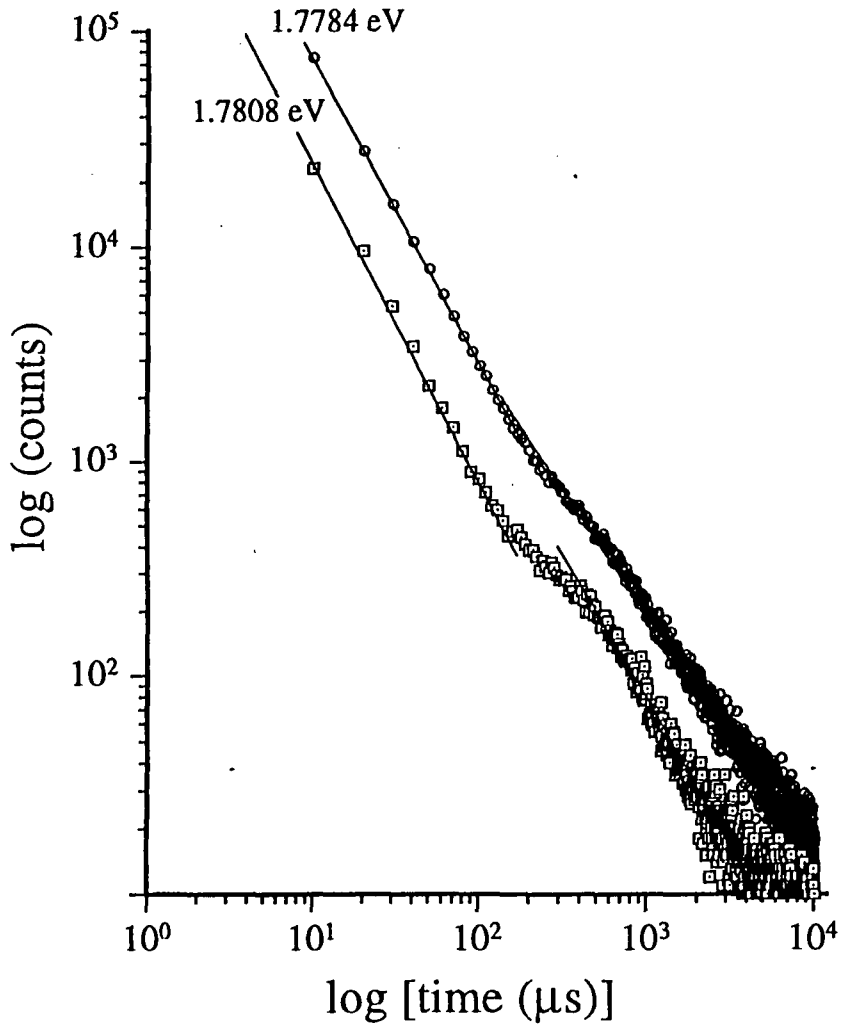
1.7784 eV
1.7808 eV
log (counts)
10^5
10^4
10^3
10^2
10^0
10^1
10^2
10^3
10^4
log [time (μs)]

Fig 9

Fig. 9